



Effect of Pressure Gradient on Local Excitation of Boundary-layer Instability Due to Free-stream Turbulence and Micro Surface Roughness

L. Shen and C. Lu [†]

School of Marine Sciences, Nanjing University of Information Science & Technology, Nanjing 210044, China

[†] *Corresponding Author Email: cglu@nuist.edu.cn*

(Received August, 24 2020; accepted December 12, 2020)

ABSTRACT

The prediction and control of the laminar-turbulent transition is crucial to the designs of vehicles, turbines, etc. The initial condition of transition depends on the exciting process of boundary-layer instability, which is the key to implement its prediction and control. The current researches confirm that the exciting process of boundary-layer instability, namely receptivity, is affected not only by different types of free-stream disturbances and shape parameters of surface roughness elements, but also by the pressure gradient of mean flow. Hence, we study the effect of pressure-gradient on local excitation of boundary-layer instability under the interaction of the low-level, isotropic free-stream turbulence and micro surface roughness in this work. The numerical results reveal the pressure-gradient effect on the receptive process and the group speed of excited wave packets in the Falkner-Skan boundary layer. The favorable/adverse pressure gradients (FPG/APG) are found to be able to promote/suppress the excitation and subsequent evolution of Tollmien-Schlichting (T-S) waves. Then the relations of the pressure gradient with the amplitude, growth rate, wave number, phase speed and shape function of excited T-S waves are studied.

Keywords: Receptivity; Pressure gradient; Boundary layer; Roughness element.

1. INTRODUCTION

The excitation of instability in the boundary layer by external disturbances, namely receptivity, is the initial stage of laminar-turbulent transition. It is well known that the transition routine highly depends on the external disturbances. At a high-level turbulence intensity, a bypass transition will be triggered. (Saric *et al.* 2002; Jacobs and Durbin 2001; Xu *et al.* 2016) Meanwhile, at a relatively low-level turbulence intensity, it will experience a linear growth stage before the nonlinear regime. And its receptive process can generally fall into two categories, i.e., leading-edge receptivity and local receptivity. The former is induced by disturbances in the free stream near the leading-edge region where non-parallelism is significant, while the latter is triggered by the interaction between free-stream disturbances and localized or distributed surface non-uniformity, e.g., roughness element, blowing or suction. (Saric *et al.* 2002; Wu 2001b; Choudhari 1993)

The mechanism of leading-edge receptivity was firstly revealed by Goldstein (1983) who employed asymptotic analysis to investigate receptivity at the

first neutral point of T-S instability in Blasius boundary layer. Then, for local receptivity, Ruban (1984) and Goldstein (1985) showed the receptive process of an unstable T-S waves due to the interaction of the acoustic waves with two-dimensional wall roughness by the triple-deck theory. This acoustic receptive theory was verified by the following experiments of Saric *et al.* (1991) and Wiegel and Wlezien (1993). On the other hand, the existence of vortical local receptivity was confirmed by Dietz (1999) experimentally in a flatplate boundary layer, where the unstable T-S waves were excited by the interaction between the freestream vortices and two-dimensional micro surface roughness. By applying the triple-deck theory, Duck *et al.* (1996) and Wu (2001a) showed that the stationary perturbations induced by surface roughness interact with the vortical oscillations in the upper deck leading to T-S wave generation. And, Wu (2001a)'s asymptotic solutions agreed well with the experimental data of Dietz (1999), including the relationship of receptivity with the amplitude of free-stream vortices, the shape, position and number of the localized roughness elements. The case of three-dimensional roughness element is studied by Würz *et al.* (2003) experimentally and numerically to interact with

oncoming acoustic waves. As a result, three-dimensional T-S waves were found to propagate downstream in a fan-shape, and the receptivity coefficient was a function of spanwise wave number and frequency of forcing wave.

The current researches have already determined the relationship between the local boundary-layer receptivity and the parameters of forcing disturbances, e.g., free-stream amplitude, the shape, position and number of the surface roughness elements at a zero pressure gradient (ZPG) condition. However, the pressure gradient of mean flow driven by the inviscid slip velocity, which is not zero in actual surfaces of vehicles, has a considerable effect on boundary-layer receptivity that cannot be neglected (Saric *et al.* 2002). And recently, via numerical simulations, Johnson and Pinarbasi (2014) found the growths of the excited T-S waves in the boundary layer depend on the pressure gradient. Meanwhile, there are few (if any) of studies about the effect of the pressure gradient on such local boundary-layer receptivity. Therefore, the present work is devoted to filling this gap by using direct numerical simulation, which is associated with the interaction of low-level free-stream turbulence and micro surface roughness. Such a study will contribute to improving the prediction of the laminar-turbulent transition.

2. FORMULATION

2.1 Scalings and Governing Equations

We consider the exciting process of unsteady instability by small-amplitude, isotropic free-stream turbulence interacting with a micro surface roughness element in a pressure-gradient boundary layer. The incompressible flow is described in a two-dimensional Cartesian system normalized by

$$(x, y) = (x^*, y^*) / \delta^*, \quad (1)$$

where δ^* is the displacement boundary-layer thickness at the inlet boundary which is located very close to the leading edge of flat plate. And the velocity, time and pressure are dimensionless by

$$\begin{cases} U_B = (U_B^*, V_B^*) / U_\infty^*, \\ \mathbf{u} = (u^*, v^*) / U_\infty^*, \\ t = t^* U_\infty^* / \delta^*, \\ p = p^* / (\rho^* U_\infty^{*2}), \end{cases} \quad (2)$$

where U_∞^* is the streamwise far-field velocity at the inlet boundary. $U_B = (U_B, V_B)$ is the base flow velocity, and $\mathbf{u} = (u, v)$ is the perturbed velocity. t, p and ρ are time, pressure, and density respectively. The variables noted by asterisk superscripts are the dimensional quantities, while those without asterisk superscripts are the corresponding dimensionless quantities.

For convenience of comparison among the cases in adverse pressure gradient (APG), zero pressure gradient (ZPG) and favorable pressure gradient (FPG), Falkner-Skan similarity solution with far-field velocity $U_e = x^m$ is introduced here to give the distributions of base flow velocity U_B in pressure-gradient boundary layers,

$$\frac{d^3 F}{d\eta^3} + F \frac{d^2 F}{d\eta^2} + \beta_H [1 - (\frac{dF}{d\eta})^2] = 0, \quad (3)$$

$$\begin{cases} U_B = U_e F_\eta, \\ V_B = -\sqrt{\frac{U_e}{2xRe}} [F - F_\eta \eta + m(F + F_\eta \eta)], \end{cases} \quad (4)$$

where the similarity variable $\eta = y\sqrt{U_e/x}$, and $\beta_H = 2m/(1+m)$ is the pressure-gradient coefficient. $\beta_H > 0$ for FPG, $\beta_H = 0$ for ZPG, and $\beta_H < 0$ for APG. The Reynolds number is defined as $Re = (U_\infty^* \delta^*) / \nu^*$, where ν^* is the kinematic viscosity coefficient. The perturbed velocity, of the external disturbances and excited instability, is governed by the nonlinear perturbation form of incompressible Navier-Stokes equations

$$\begin{cases} \nabla \cdot \mathbf{u} = 0, \\ \frac{\partial \mathbf{u}}{\partial t} + (U_B \cdot \nabla) \mathbf{u} + (\mathbf{u} \cdot \nabla) U_B + (\mathbf{u} \cdot \nabla) \mathbf{u} \\ = -\nabla p + \frac{1}{Re} \nabla^2 \mathbf{u}. \end{cases} \quad (5)$$

The excitation of the boundary layer instability, namely Tollmien-Schlichting waves, have to involve the interaction between the unsteady disturbances in the free stream and the steady inhomogeneities on the surface of the flat plate, which is a nonlinear process. However, after the exciting regime, the subsequent development of the unstable waves is almost linear due to their small amplitudes. In this regime, the wave-wave interactions are rather small that cannot affect the growth rate at the leading order.

In order to solve the governing equations Eq. (5) numerically, a modified fourth-order Runge-Kutta scheme is introduced for the temporal march, and compact finite difference schemes on nonuniform meshes are applied for the spatial derivatives, i.e., fifth-order upwind schemes for the convective terms, sixth-order symmetric schemes for the pressure-gradient terms, and fifth-order symmetric schemes for the viscosity terms. The pressure equations are solved by third-order iterative scheme. See Shen and Lu (2016), Shen and Lu (2017), Shen and Lu (2018), Shen *et al.* (2019), Shen and Lu (2021) for the details of the discretization and validation.

2.2 Model of Free-Stream Turbulence

A proper mathematical model to formulate freestream turbulence for inlet and far-field

boundary conditions is vital to the calculation. Accounting for the randomness of turbulence and satisfying the continuity equation, a mathematical model in Fourier modes proposed by [Jacobs and Durbin \(2001\)](#) is adopted here to describe the oncoming turbulence in the free stream, which can be written in a two-dimensional form,

$$u_\infty = \delta \sum_{m=-M}^M \sum_{j=-J}^J \begin{pmatrix} \hat{u}_\infty \\ \hat{v}_\infty \end{pmatrix} \cdot e^{I[m\kappa_1(x-t) + j\kappa_2 y]}, \quad (6)$$

where

$$\begin{cases} \hat{u}_\infty(m, j) = I \frac{m\kappa_1 j\kappa_2}{\kappa \sqrt{m^2 \kappa_1^2}} \cdot \sqrt{\frac{2E(\kappa)\kappa_1\kappa_2}{4\pi\kappa^2}} \cdot e^{I\sigma}, \\ \hat{v}_\infty(m, j) = -I \frac{\sqrt{m^2 \kappa_1^2}}{\kappa} \cdot \sqrt{\frac{2E(\kappa)\kappa_1\kappa_2}{4\pi\kappa^2}} \cdot e^{I\sigma}. \end{cases} \quad (7)$$

Here $I = \sqrt{-1}$, u_∞ and v_∞ are the streamwise and normal components of perturbed velocity of free-stream turbulence respectively. \hat{u}_∞ and \hat{v}_∞ are the spectra of u_∞ and v_∞ related to the energy spectrum $E(\kappa)$ and random phase angle σ . δ denotes the amplitude. M and J are the maximum mode numbers. κ_1 and κ_2 are the fundamental wave numbers in the x - and y -directions respectively, and $\kappa = \sqrt{m^2 \kappa_1^2 + j^2 \kappa_2^2}$. The streamwise and normal wave numbers are $\alpha = m\kappa_1$ and $\gamma = j\kappa_2$.

2.3 Computational Domain and Boundary Conditions

Figure 1 gives the computational domain of the present work. The streamwise length is 1000, and the normal length is six times of the boundary layer thickness at the inlet boundary 17.26. The computational meshes are 512×200 grids in the x - and y -directions. Non-uniform meshes are utilized in the normal direction so that the grids can be refined in the near-wall region. The Reynolds number is set to be 1000.

The far-field boundary: The velocities are given by the free-stream turbulence model Eq. (6) and $p=0$.

The wall boundary: The no-slip condition is utilized, i.e., $u = v = 0$, and $\partial p / \partial y = 0$. As the height of micro roughness element is very small, it can be equivalent to the localized velocities by linear treatment ([Iuchini 2013](#)),

$$u(x, 0) = -h(x) \cdot U_{B,\eta}(0), \quad (8)$$

where $h(x)$ is the roughness height. $U_{B,\eta}(0)$ is the first normal derivative of base flow velocity at the wall.

The inlet boundary: The velocities are given by the free-stream turbulence model Eq. (6), and $\partial p / \partial x = 0$.

The outlet boundary: The velocities are computed by the $\overline{u_{\text{FST}}^2}$ non-reflect boundary condition [Shen and Lue \(2016\)](#). And the computation is terminated before the excited waves reach the outlet boundary.

3. Results and Discussion

The mechanism of local receptivity to free-stream turbulence in the Blasius boundary layer has been already revealed by [Duck et al. \(1996\)](#), [Wu \(2001a\)](#), [Dietz \(1999\)](#). Therefore, in this paper, we focus on the pressure gradient effect on the excitation of T-S instability. In this case, a rectangle roughness elements is placed at $x \in [150, 200]$ with a height of $h = 0.01$ that is very small comparable with the boundary-layer thickness. The fundamental wave number of imposed free-stream turbulence is $\kappa_1 = 0.010$ with $M=8$. The turbulence intensity $A_{\text{FST}} = (\overline{u_{\text{FST}}^2} + \overline{v_{\text{FST}}^2})^{1/2} = 0.5\%$ is sufficient low to avoid nonlinear interaction in the free stream, where and $\overline{v_{\text{FST}}^2}$ are the mean square roots of the perturbed velocities at the outer edge of boundary layer.

3.1 Validation of Numerical Settings

Before the simulation of the excitation of boundary-layer instability, the numerical settings including the numerical method and generated mesh. The computational mesh is shown in Fig. 2(a) which is clustered near the wall and most of the grids are placed inside the boundary layer. And the first and second derivatives dy/dj and d^2y/dj^2 of the y -grids are given in Fig. 2(b), where $j \in [1, Jmax]$ is the index of the grids in the normal direction. Both the first and second derivatives of the y -grids are smooth function so that ensuring the stable calculation on this mesh.

The eigenmodes in a Blasius boundary layer with various **wavenumbers** α_{os} , including the shortest wavelength of the unstable wave in the simulation, obtained by the Orr-Sommerfeld equation are imposed at the inlet boundary and to travel downstream in order to verify the convergence of the mesh. The relative errors of the dispersion relations (complex streamwise wavenumber α) of the eigenmodes at downstream location $x=800$ between numerical results on different streamwise meshes and theoretical solutions from Orr-Sommerfeld equation are shown in Fig. 3. The real part α_r associated with the wavelength and its relative error represents the disperse error, and imaginary part α_i associated with the growth rate and its relative error represents the dissipative error. Apparently, fine meshes (2024, 1024 and 512 streamwise-grids) give relatively exact results for both the real part and imaginary part of the

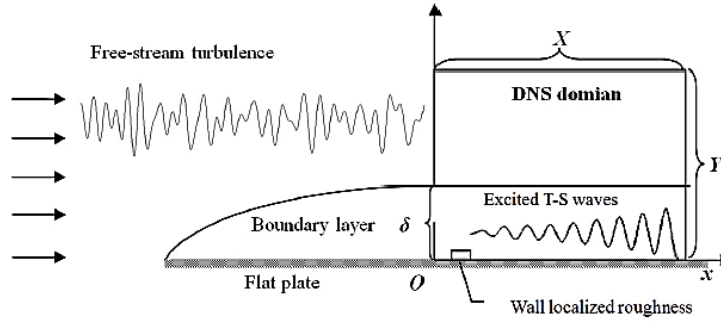


Fig. 1. Computational domain.

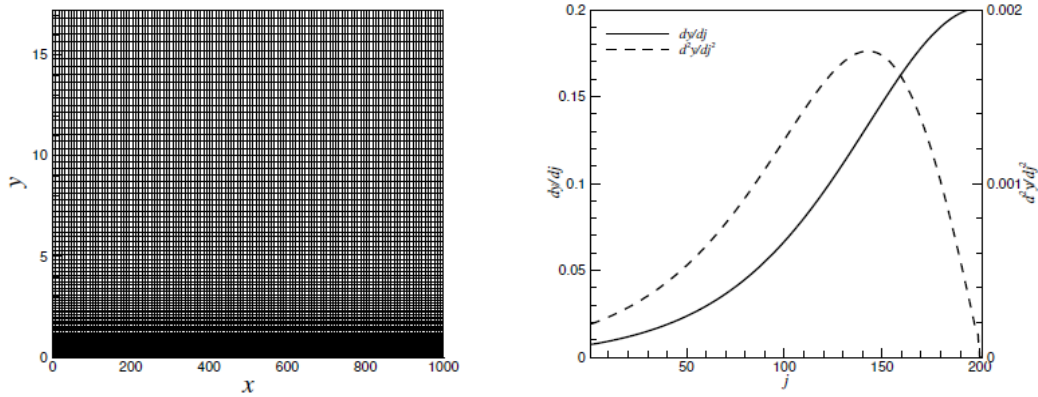


Fig. 2. (a) Sketch of computational mesh and (b).

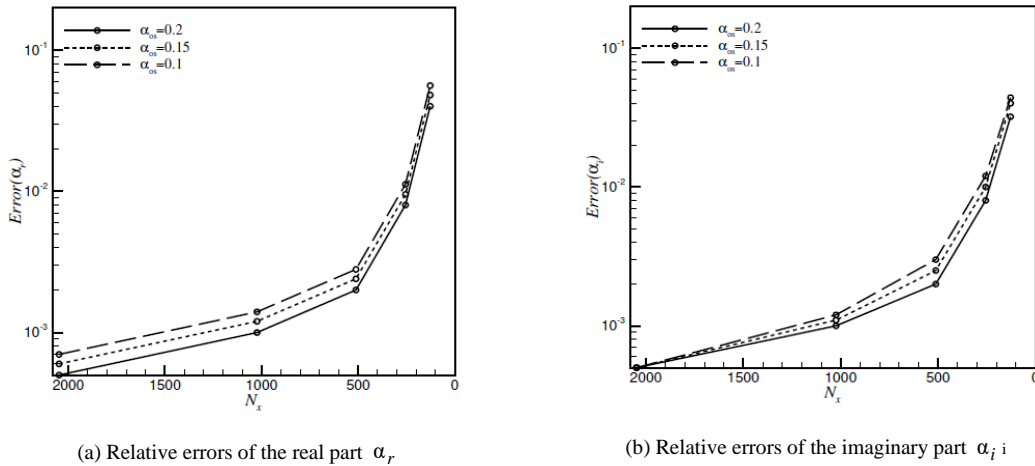


Fig. 3. Relative errors of the complex streamwise wavenumber α of the eigenmodes on different streamwise meshes at $x = 800$.

wavenumber α . And the course meshes having less than 512 streamwise-grids bring in a visible errors for the unstable waves. In view of this, we choose a mesh of 512 streamwise-grids for the efficiency of computation.

First and second derivatives dy/dj and d^2y/dj^2 of the y -grid in the normal direction.

3.2 Excitation of Wave Packets

Due to the interaction of free-stream turbulence and surface roughness, small-amplitude wave packets is observed as expected in the downstream of roughness element. Figure 4 gives the streamwise evolution of streamwise velocity of the excited T-S wave packets in typical FPG, ZPG and

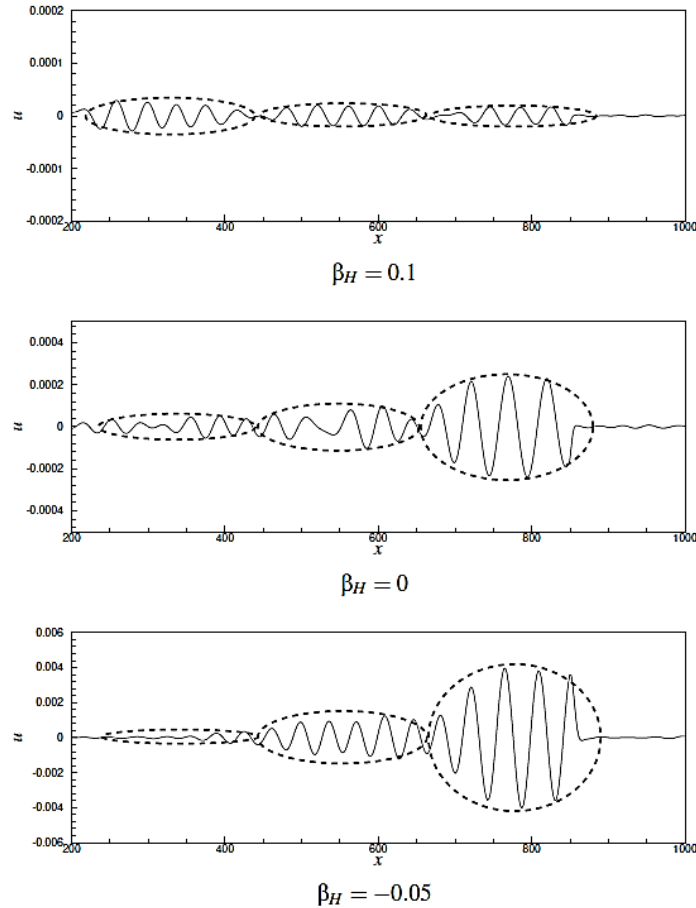


Fig. 4. Streamwise evolution of streamwise velocity of the excited T-S wave packets in various pressure-gradient boundary layers. ($y = 0.66$, $t = 2500$)

APG boundary layers separately at $y=0.66$. The pressure-gradient effect is apparent. The excited wave packets in ZPG ($\beta_H = 0$) and APG ($\beta_H = -0.05$) are amplifying as it propagates downstream, and those in FPG ($\beta_H = 0.1$), in contrast, is decaying downstream.

By recording the positions of the antinodes of the wave packets at different times, the average group speeds are approximately calculated, as shown in table 1. The group speed decreases very slightly as pressure gradient coefficient β_H decreases.

One of the main targets for the study of boundary-layer receptivity is to determine the initial amplitude of the instability which provides the initial condition for the prediction of laminar-turbulent transition. (Dietz 1999; Saric *et al.* 2002) Hence, the initial amplitude of the excited wave

packets A_R is calculated and compared in this section. The initial amplitude A_R is defined as $A_R = (\overline{u_R^2} + \overline{v_R^2})^{1/2}$, where $\overline{u_R^2}$ and $\overline{v_R^2}$ are the mean squares of the perturbed velocities of the excited wave packets at the roughness location which is calculated by extrapolation of the downstream amplitude. Figure 5 gives the initial amplitudes of the excited T-S wave packets with the different pressure-gradient coefficients β_H . It shows that the initial amplitude A_R slowly increases as the pressure-gradient coefficient β_H decreases from favorable to adverse. And the greater APG (absolute value of pressure-gradient coefficient $|\beta_H|$) corresponds to larger initial amplitude, namely stronger receptivity, and opposite result is obtained for FPG.

Table G group speeds C_g of excited wave packets in various pressure-gradient boundary layers.

β_H	0.3	0.1	0.05	0	-0.05	-0.1
C_g	0.357	0.347	0.342	0.334	0.332	0.330

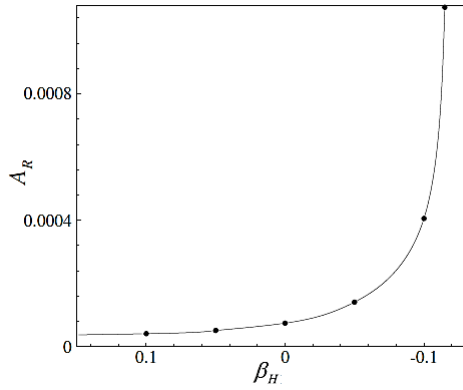


Fig. 5. Variation of the initial amplitude of the excited T-S wave packets A_R with the pressure-gradient coefficient β_H .

3.3 Separated T-S Waves

Subsequently, by using fast Fourier transform, the streamwise evolution of excited T-S waves with the frequencies $F=40$ and $F=60$ are extracted from the wave packets. Due to the small amplitudes of the excited waves, the subsequent development is almost linear and the wave-wave interactions are rather small that cannot affect the growth rate at the leading order. The results of FPG and APG are compared with the numerical results of ZPG ($\beta_H = 0$), i.e., those results from Shen and Lu (2016), Shen and Lu (2018). And the numerical results are also compared with the linear stability theory, which is based on Orr-Sommerfeld equation, to identify and analysis the generated unstable waves. The distributions of streamwise velocity of separated waves along x -direction at $y = 0.66$ are shown in Fig. 6. The left y -axis scale is for the cases of FPG and ZPG, and the right y -axis scale is for the case of APG. The non-dimensional frequency is defined as $F = 2\pi f\nu / U_\infty^2 \times 10^6$. At $F=40$ (Fig. 6(a)), an unstable T-S wave is excited in the ZPG boundary layer, and a more unstable T-S wave with larger growth rate is excited by APG. In contrast, FPG

suppress the growth of the T-S wave which is unstable in ZPG, and transforms it to a stable one. At $F=60$ (Fig. 6(b)), we can observe a stable T-S wave in ZPG, and a more stable T-S wave with larger decaying rate in FPG. Conversely, an unstable T-S wave is found in APG. The above observations demonstrate that APG is able to significantly enhance the receptive process, whereas FPG weakens the process.

The average streamwise wave numbers and phase speeds of the excited waves can also be calculated, according to their spatial evolution in pressure-gradient boundary layers. The obtained results are shown in Table 2. It is clearly seen that as the pressure-gradient coefficient β_H increases, the real part of streamwise wave number α_r of excited T-S waves with same frequency decreases gradually, and phase speed C increases. This means that for larger pressure-gradient coefficient β_H , the excited waves have longer wavelength and travel faster in the streamwise direction.

Further studies were made of the effect of the pressure gradient on the initial amplitude and growth rate of the excited T-S waves. Similarly, the amplitude of T-S waves is defined as

$A_{TS} = (\overline{u_{TS}^2} + \overline{v_{TS}^2})^{1/2}$, where $\overline{u_{TS}^2}$ and $\overline{v_{TS}^2}$ are the mean squares of the velocity of T-S waves. The amplitudes near the roughness element including the initial amplitude are calculated by extrapolation of the downstream amplitude.

Figures 7 and 8 give the streamwise evolution of the amplitude A_{TS} and growth rate $-\alpha_i$ of the excited T-S waves with multiple frequencies in typical pressure-gradient boundary layers. At $F=40$, the APG transforms an unstable T-S mode into a more unstable T-S mode with greater growth rate. This T-S mode amplifies downstream, and its growth rate keeps positive and greater than those in ZPG. On the contrary, FPG converts an unstable T-S mode into a stable one. This T-S mode decreases quickly and the growth rate remains negative and smaller than those in ZPG. The

Table Streamwise wave numbers α_r and phase speeds C of excited waves in various pressure-gradient boundary layers (α_r, C).

β_H	-0.1	-0.05	0	0.05	0.1
F=30	(0.0975,0.3078)	(0.0962,0.3119)	(0.0947,0.3168)	(0.0932,0.3220)	(0.0916,0.3275)
F=40	(0.1264,0.3165)	(0.1252,0.3195)	(0.1237,0.3234)	(0.1219,0.3281)	(0.1200,0.3334)
F=50	(0.1537,0.3254)	(0.1525,0.3278)	(0.1512,0.3307)	(0.1492,0.3351)	(0.1470,0.3401)
F=60	(0.1796,0.3340)	(0.1787,0.3358)	(0.1774,0.3382)	(0.1756,0.3417)	(0.1733,0.3462)
F=70	(0.2049,0.3417)	(0.2038,0.3434)	(0.2025,0.3456)	(0.2011,0.3481)	(0.1989,0.3519)
F=80	(0.2291,0.3492)	(0.2282,0.3505)	(0.2271,0.3523)	(0.2256,0.3546)	(0.2240,0.3571)

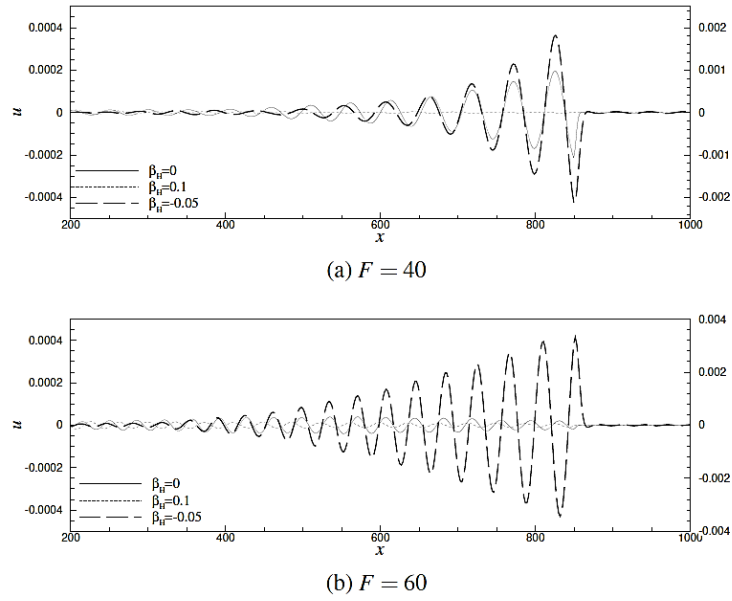


Fig. 6. Streamwise evolution of the excited T-S wave in various pressure-gradient boundary layers. ($y = 0.66, t = 2500$)

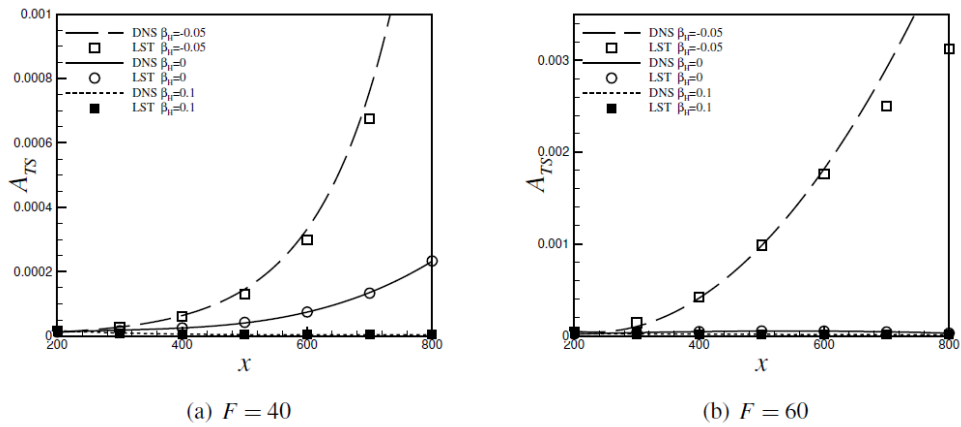


Fig. 7. Streamwise evolution of the amplitudes of excited waves A_{TS} in various pressure-gradient boundary layers.

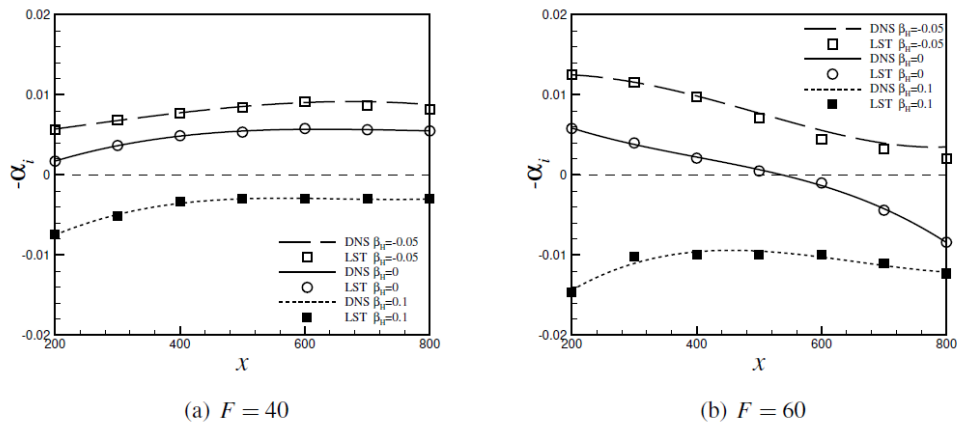


Fig. 8. Streamwise evolution of the growth rates of excited waves $-\alpha_i$ in various pressure-gradient boundary layers.

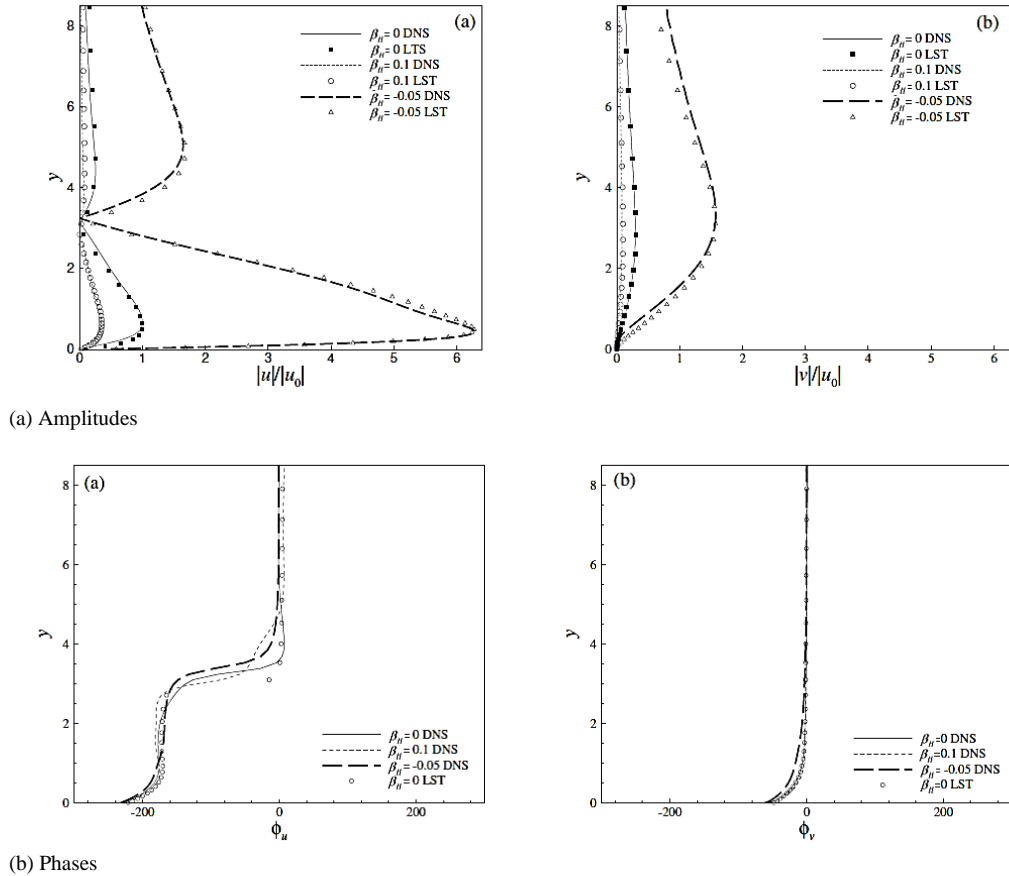


Fig.9. Profiles of the amplitude and phase of the shape functions of the excited T-S waves in various pressure-gradient boundary layers. ($x = 450$)

numerical results agree well with those of e^N method and linear stability theory (LST) (Shen and Lu 2016; Shen and Lu 2018). At $F = 60$, APG transforms a stable T-S mode into an unstable one. It grows fast downstream with positive growth rate which is greater than those in ZPG. And FPG induce a more stable wave. Particularly, the results in APG deviate from those of e^N method and linear stability theory in the downstream region, because the excited T-S amplitude is one order greater than that of $F = 40$, thus introduces significant nonlinear effect.

The excited T-S waves of $F = 40$ is chosen to show the profiles of the amplitude and phase of the shape functions. The wave amplitudes in Fig. 9 are normalized by the maximum amplitude of streamwise velocity of T-S waves in the ZPG boundary layer $|u_0|$. The shapes of amplitude profiles (Fig. 9(a)) in different pressure-gradient boundary layers are identical. But the amplitudes of the excited T-S waves in the APG boundary layer are obviously greater than those in the FPG and ZPG boundary layers. Moreover, the profile of the phase (Fig. 9(b)) in different pressure-gradient boundary layers match well, and agree with the eigenfunction of linear stability theory (Shen and Lu 2016; Shen and Lu 2018). It indicates that the

shape functions of amplitude and phase of excited T-S waves are not changed by pressure-gradient effect.

4. Conclusions

A direct numerical simulation was performed to study the effect of pressure gradient of mean flow on boundary-layer receptivity due to the interaction of Low-level, isotropic free-stream turbulence and a rectangle micro roughness upon a flat plate. For convenience of comparison among the cases in APG, ZPG and FPG, Falkner-Skan similarity solution is introduced to produce the pressure-gradient boundary layers.

The pressure-gradient effect on the excitation of wave packets is apparent. The excited wave packets in ZPG and APG are amplifying as it propagates downstream, and those in FPG is decaying downstream. The group speed decreases very slightly as pressure gradient coefficient β_H decreases. The initial amplitude A_R of excited wave packets slowly increases as the pressure-gradient coefficient β_H decreases from favorable to adverse.

T-S waves are extracted from the wave packets by using fast Fourier transform. The observations of

the separated T-S waves in different pressure-gradient boundary layers demonstrate that APG is able to significantly enhance the receptive process, whereas FPG weakens the process. For larger pressure-gradient coefficient β_H , the excited T-S waves have longer wavelength and faster propagation speeds. And the dispersion relations of excited T-S waves agree well with the results of linear stability theory. Moreover, APG can promote the growth of excited T-S waves, whereas FPG suppresses the growth of the excited T-S waves. The profiles of amplitude and phase of the excited T-S waves in different pressure-gradient boundary layers are similar. However, the amplitude profile in APG are obviously greater than those in FPG or ZPG. And the shape functions of amplitude and phase of excited T-S waves are not changed by pressure-gradient effect.

ACKNOWLEDGMENTS

This project is supported by the National Natural Science Foundation of China (No.11802143) and the Natural Science Foundation of Jiangsu Province, China (No.BK20180781).

REFERENCES

- Choudhari, M. (1993). Boundary-layer receptivity due to distributed surface imperfections of a deterministic or random nature. *Theoretical and Computational Fluid Dynamics* 4(3), 101–117.
- Dietz, A. (1999). Local boundary-layer receptivity to a convected free-stream disturbance. *Journal of Fluid Mechanics* 378, 291–317.
- Duck, P., A. Ruban and C. Zhikharev (1996). The generation of tollmien-schlichting waves by free-stream turbulence. *Journal of Fluid Mechanics* 312, 341–371.
- Goldstein, M. (1983). The evolution of tollmien-schlichting waves near a leading edge. *Journal of Fluid Mechanics* 127, 59–81.
- Goldstein, M. E. (1985). Scattering of acoustic waves into tollmien-schlichting waves by small streamwise variations in surface geometry. *Journal of Fluid Mechanics* 154, 509 - 529.
- Jacobs, R. and P. Durbin (2001). Simulations of bypass transition. *Journal of Fluid Mechanics* 428, 185.
- Johnson, M. W. and A. Pinarbasi (2014). The effect of pressure gradient on boundary layer receptivity. *Flow, turbulence and combustion* 93(1), 1–24.
- Luchini, P. (2013). Linearized no-slip boundary conditions at a rough surface. *Journal of fluid mechanics* 737, 349.
- Ruban, A. (1984). On the generation of tollmienschlichting waves by sound. *Fluid Dynamics* 19(5), 709–717.
- Saric, W. S., J. A. Hoos and R. H. Radeztsky (1991). Boundary-layer receptivity of sound with roughness. *Boundary Layer Stability and Transition to Turbulence*, 17–22.
- Saric, W. S., H. L. Reed and E. J. Kerschen (2002). Boundary-layer receptivity to freestream disturbances. *Annual review of fluid mechanics* 34(1), 291–319.
- Shen, L. and C. Lu (2016). Boundary-layer receptivity under interaction of free-stream turbulence and localized wall roughness. *Applied Mathematics and Mechanics* 37(3), 349–360.
- Shen, L. and C. Lu (2017). Mechanism of three-dimensional boundary-layer receptivity. *Applied Mathematics and Mechanics* 38(9), 1213–1224.
- Shen, L. and C. Lu (2018). A boundary-layer receptivity mechanism excited by the interaction between free-stream turbulence and the three-dimensional localized wall roughness. *Advances in Applied Mathematics and Mechanics* 10(3), 735–751.
- Shen, L. and C. Lu (2021). Effect of leadingedge curvature on receptivity of stationary cross-flow modes in swept-plate boundary layers. *Advances in Applied Mathematics and Mechanics* 13(2), 467-480.
- Shen, L., C. Lu and X. Zhu (2019). Leadingedge receptivity of boundary layer to three-dimensional free-stream turbulence. *Applied Mathematics and Mechanics* 40(6), 851– 860.
- Wiegel, M. and R. Wlezien (1993). Acoustic receptivity of laminar boundary layers over wavy walls. In *3rd Shear Flow Conference*, pp. 3280.
- Wu, X. (2001a). On local boundary-layer receptivity to vortical disturbances in the free stream. *Journal of Fluid Mechanics* 449, 373.
- Wu, X. (2001b). Receptivity of boundary layers with distributed roughness to vortical and acoustic disturbances: a second-order asymptotic theory and comparison with experiments. *Journal of Fluid Mechanics* 431, 91.
- Würz, W., S. Herr, A. Wörner, U. Rist, S. Wagner and Y. S. Kachanov (2003). Three-dimensional acoustic-roughness receptivity of a boundary layer on an airfoil: experiment and direct numerical simulations. *Journal of Fluid Mechanics* 478, 135–163.
- Xu, J., J. Bai, L. Qiao and Y. Zhang (2016). Correlation-based transition transport modeling for simulating crossflow instabilities. *Journal of Applied Fluid Mechanics* 9(5).

